Intestinal Epithelial Cell Tyrosine Kinase 2 Transduces IL-22 Signals To Protect from Acute Colitis

Eva Hainzl,[*,1] Silvia Stockinger,[*,1] Isabella Rauch,[†,‡] Susanne Heider,[§] David Berry,[¶] Caroline Lassnig,[*,‖] Clarissa Schwab,[#] Felix Rosebrock,[†] Gabriel Milinovich,[#] Michaela Schlederer,[§] Michael Wagner,[¶] Christa Schleper,[#] Alexander Loy,[¶] Tim Urich,[#] Lukas Kenner,[§,,††] Xiaonan Han,[‡‡] Thomas Decker,[†] Birgit Strobl,[*] and Mathias Müller[*,‖]**

In the intestinal tract, IL-22 activates STAT3 to promote intestinal epithelial cell (IEC) homeostasis and tissue healing. The mechanism has remained obscure, but we demonstrate that IL-22 acts via tyrosine kinase 2 (Tyk2), a member of the Jak family. Using a mouse model for colitis, we show that *Tyk2* deficiency is associated with an altered composition of the gut microbiota and exacerbates inflammatory bowel disease. Colitic *Tyk2*$^{-/-}$ mice have less p-STAT3 in colon tissue and their IECs proliferate less efficiently. *Tyk2*-deficient primary IECs show reduced p-STAT3 in response to IL-22 stimulation, and expression of IL-22–STAT3 target genes is reduced in IECs from healthy and colitic *Tyk2*$^{-/-}$ mice. Experiments with conditional *Tyk2*$^{-/-}$ mice reveal that IEC-specific depletion of Tyk2 aggravates colitis. Disease symptoms can be alleviated by administering high doses of rIL-22–Fc, indicating that *Tyk2* deficiency can be rescued via the IL-22 receptor complex. The pivotal function of Tyk2 in IL-22–dependent colitis was confirmed in *Citrobacter rodentium*–induced disease. Thus, Tyk2 protects against acute colitis in part by amplifying inflammation-induced epithelial IL-22 signaling to STAT3. ***The Journal of Immunology*****, 2015, 195: 5011–5024.**

The Jak/STAT signaling pathway conveys extracellular signals from transmembrane receptors to the nucleus, where transcription of target genes is initiated. Tyrosine kinase 2 (Tyk2) is a member of the Jak family and has been described to participate in signaling of cytokines such as type I IFN, IL-10, IL-12, IL-13, and IL-6 family members. *Tyk2*-deficient mice are highly susceptible to viral, bacterial, and parasitic infections, which are mainly due to a diminished type I IFN response and an impaired IL-12–dependent IFN-γ production (1). Owing to their altered Th1/Th2, Th9, and Th17 cytokine profiles, these mice are more prone to allergic airway inflammation (2, 3). Alternatively, *Tyk2*-null mice are more resistant to autoimmune diseases (4, 5). In humans, *Tyk2* deficiency has been demonstrated to affect signaling of type I IFNs, IL-6, IL-10, IL-12, and IL-23, leading to increased susceptibility to infections and inflammatory symptoms (6, 7).

Cytokines and their respective signaling pathways regulate intestinal homeostasis, and pro- and anti-inflammatory cytokines, including the Tyk2-dependent IFNs, IL-6, IL-10, IL-12, IL-22, IL-23, and IL-27, may have beneficial or detrimental roles in a colitogenic environment (8). In a screen for susceptibility factors in inflammatory bowel disease (IBD), polymorphisms in the *Tyk2* and *Stat3* loci were found (9). We recently identified that IFN-I and IFN-III signals are involved in the progression and resolution of colitis (10, 11). Several reports, including our recent findings, demonstrate a proinflammatory function of IFN-γ (11, 12) whose expression is known to be severely reduced in immunologically challenged *Tyk2*$^{-/-}$ mice (1). Also, IL-12 and IL-23 were shown to have a key pathogenic role in colitis development whereas IL-10 and IL-22 are considered to prevent disease (8). Besides the cytokine milieu, multiple factors such as epithelial barrier defects and altered microbiota composition contribute to the complex etiology seen in IBD (13, 14).

In this study, we characterized the role of Tyk2 in intestinal inflammation in various colitis models. Furthermore, influences of *Tyk2* deletion on cytokine expression and response in the intestine were analyzed. A comprehensive intestinal microbiota analysis employing 16S rRNA gene-targeted amplicon sequencing and metatranscriptomics was performed to elucidate the impact of dextran sodium sulfate (DSS)–induced colitis in wild-type (WT)

*Institute of Animal Breeding and Genetics, University of Veterinary Medicine, Vienna, 1210 Vienna, Austria; [†]Max F. Perutz Laboratories, University of Vienna, 1030 Vienna, Austria; [‡]Department of Molecular and Cell Biology, University of California, Berkeley, Berkeley, CA 94720; [§]Ludwig Boltzmann Institute for Cancer Research, 1090 Vienna, Austria; [¶]Department of Microbiology and Ecosystem Science, University of Vienna, 1090 Vienna, Austria; [‖]Biomodels Austria, University of Veterinary Medicine, Vienna, 1210 Vienna, Austria; [#]Department of Ecogenomics and Systems Biology, University of Vienna, 1090 Vienna, Austria; **Institute for Clinical Pathology, Medical University Vienna, 1090 Vienna, Austria; [††]Unit of Pathology of Laboratory Animals, University of Veterinary Medicine, Vienna, 1210 Vienna, Austria; and [‡‡]Division of Gastroenterology, Hepatology, and Nutrition, Cincinnati Children's Hospital Medical Center, Cincinnati, OH 45229

[1]E.H. and S.S. contributed equally to this work.

Received for publication October 9, 2014. Accepted for publication September 7, 2015.

This work was supported by grants from Austrian Science Fund Grants SFB-F28 (to T.D., B.S., and M.M.) and P26011 (to L.K.), Vienna Science and Technology Fund Grant LS12-001 (to A.L. and D.B.), and by a grant from the Austrian Federal Ministry of Science and Research (GEN-AU III InflammoBiota).

Address correspondence and reprint requests to Dr. Mathias Müller and Dr. Silvia Stockinger, Institute of Animal Breeding and Genetics, University of Veterinary Medicine Vienna, Veterinaerplatz 1, 1210 Vienna, Austria. E-mail addresses: mathias.mueller@vetmeduni.ac.at (M.M.) and silvia.stockinger@vetmeduni.ac.at (S.S.)

The online version of this article contains supplemental material.

Abbreviations used in this article: DSS, dextran sodium sulfate; IBD, inflammatory bowel disease; IEC, intestinal epithelial cell; m, murine; PCA, principal component analysis; pY-STAT3, tyrosine phosphorylation of STAT3; qPCR, quantitative PCR; RT-qPCR, real-time qPCR; TNBS, 2,4,6-trinitrobenzene sulfonic acid; Tyk2, tyrosine kinase 2; WT, wild-type.

and *Tyk2*$^{-/-}$ mice. We reveal a key function of Tyk2 in intestinal epithelial cells (IECs) during acute colitis by critically affecting IL-22/STAT3–dependent responses.

Materials and Methods

Animals

Tyk2$^{-/-}$, *Tyk2*$^{fl/fl}$, and *Tyk2*$^{\Delta CMV}$ mice have been described previously (15). *Tyk2*$^{fl/fl}$ mice were crossed to *Villin-cre* transgenic mice (16) to obtain *Tyk2*$^{\Delta Villin}$ mice. *Tyk2*$^{fl/fl}$ littermate mice were used as controls. All genetically engineered mice were on C57BL/6N background controlled by speed congenics (17). C57BL/6N WT controls were kept under identical housing conditions. Mice were frequently tested to be specific pathogen-free according to the recommendations of the Federation of European Laboratory Animal Science Association, and they were additionally monitored to be norovirus negative (18). All animal experiments were approved by the Institutional Ethics Committee and were conducted in accordance with Austrian laws (BMWF-66.006/0002-II/10b/2010, BMWF-66.006/0003-II/3b/2012, BMWFW-66.006/0002-WF/V/3b/2015) and were performed according to the guidelines of Federation of European Laboratory Animal Science Associations and Animal Research: Reporting In Vivo Experiments.

DSS treatment and assessment of colitis

Mice aged 8–10 wk of matched genders were treated with 2% (w/v) DSS (MP Biomedicals, molecular mass of 36,000–50,000 Da) in autoclaved tap water ad libitum for 7 d. On day 7 of treatment, mice received freshly autoclaved tap water until the experimental endpoint (19). Where indicated, mice were injected i.p. with recombinant murine (m)IL-22–Fc (50 μg/200 μl/mouse, provided by Genentech, South San Francisco, CA) (20) or IgG2A isotype control.

Upon sacrifice, intestines were removed, flushed with PBS (PAA Laboratories), and the colons were halved lengthwise. One half was frozen in liquid N_2 for RNA or protein isolation and the other half was flushed, prepared as a Swiss roll, and fixed in 2% paraformaldehyde. H&E-stained paraffin sections were imaged and used for pathological evaluation. Sections were scored blindly by a pathologist, and a histological colitis score was calculated by the sum of inflammation severity, inflammation extent, and crypt damage multiplied by the percentage of tissue area involved (21).

2,4,6-Trinitrobenzene sulfonic acid treatment and assessment of colitis

2,4,6-Trinitrobenzene sulfonic acid (TNBS) treatment was performed as described (19). Because C757BL/6 mice have been shown to be relatively resistant to TNBS colitis, a presensitization step has been included. In brief, age- and sex-matched mice were presensitized with TNBS via the skin. After 7 d, a 5% TNBS solution (Sigma-Aldrich) mixed 1:1 with 1 vol absolute ethanol was applied intrarectally. Control mice received 50% EtOH. For histology, colons were isolated on days 4 and 7 after intrarectal treatment, flushed with PBS (Sigma-Aldrich), and fixed in 7.5% formaldehyde. H&E-stained paraffin sections were imaged and used for pathological evaluation. Sections were scored by a pathologist and a histological score of colitis was assessed as: 0, no inflammation; 1, very low levels of inflammation, low level of leukocytic infiltration; 2, low level of leukocytic infiltration; 3) high level of leukocytic infiltration, high vascular density, thickening of the colon wall; 4) transmural infiltrations, loss of goblet cells, high vascular density, thickening of the colon wall (22, 23).

16S rRNA gene amplicon pyrosequencing, data analysis, and quantification of selected 16S rRNA gene copies by quantitative PCR

16S rRNA amplicon libraries were produced from DNA of cecum and colon lumen contents as described before (21). Pooled triplicate amplifications were purified (Agencourt AMPure, Beckman Coulter Genomics) and quantified with a fluorescent stain–based kit (Quant-iT PicoGreen, Invitrogen). Pyrosequencing was performed with titanium reagents on a 454 genome sequencer FLX (Roche). Pyrosequencing reads were processed as described (21). Amplicon sequencing libraries had a mean number of 17,999 reads (range, 4,415–26,495). β diversity measures were

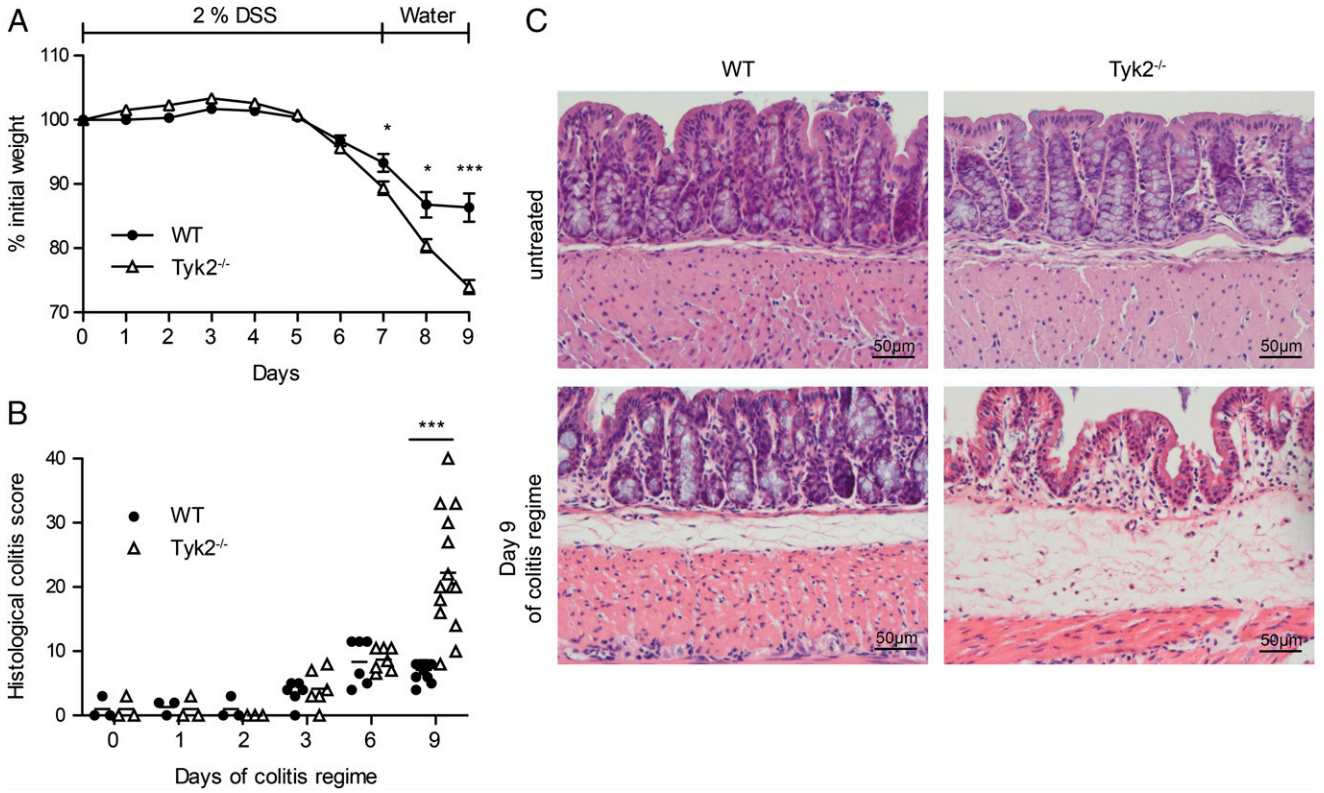

FIGURE 1. Detrimental effect of *Tyk2* deficiency on DSS-induced colitis. (**A**–**C**) C57BL/6N (WT) and *Tyk2*$^{-/-}$ mice were treated with 2% DSS for 7 d, followed by 2 d of water. (A) Weight loss was determined daily and is displayed relative to initial weight. Data are derived from five independent experiments with $n = 23$ (WT) or $n = 19$ (*Tyk2*$^{-/-}$) total. Results are given as mean values ± SEM. (B) Histological scores for days 0, 1, 2 (each $n = 3$), 3, 6 (each $n = 6$), and 9 ($n = 12$) of DSS treatment. Results for individual mice and mean values are depicted. (C) WT and *Tyk2*$^{-/-}$ colon tissue sections were stained with H&E. Representative images are shown for untreated mice and for mice on day 9 of DSS treatment. *$p < 0.05$, ***$p < 0.001$.

analyzed at 3500 reads. Quantitative PCR (qPCR) for quantitation of selected 16S rRNA genes was performed as described before (10).

Metatranscriptome sequencing and data analysis

cDNA libraries from luminal contents were prepared as described before (24) and paired-end sequenced using an Illumina genome analyzer or HiSeq (Campus Science Support Facilities, Vienna, Austria). Data were processed and analyzed as described (24).

All pyrosequencing data in the study, including amplicon and metatranscriptomic data, are available in Supplemental Table I or archived at National Center for Biotechnology Information Sequence Read Archive under accession no. SRA059289 (http://www.ncbi.nlm.nih.gov/sra).

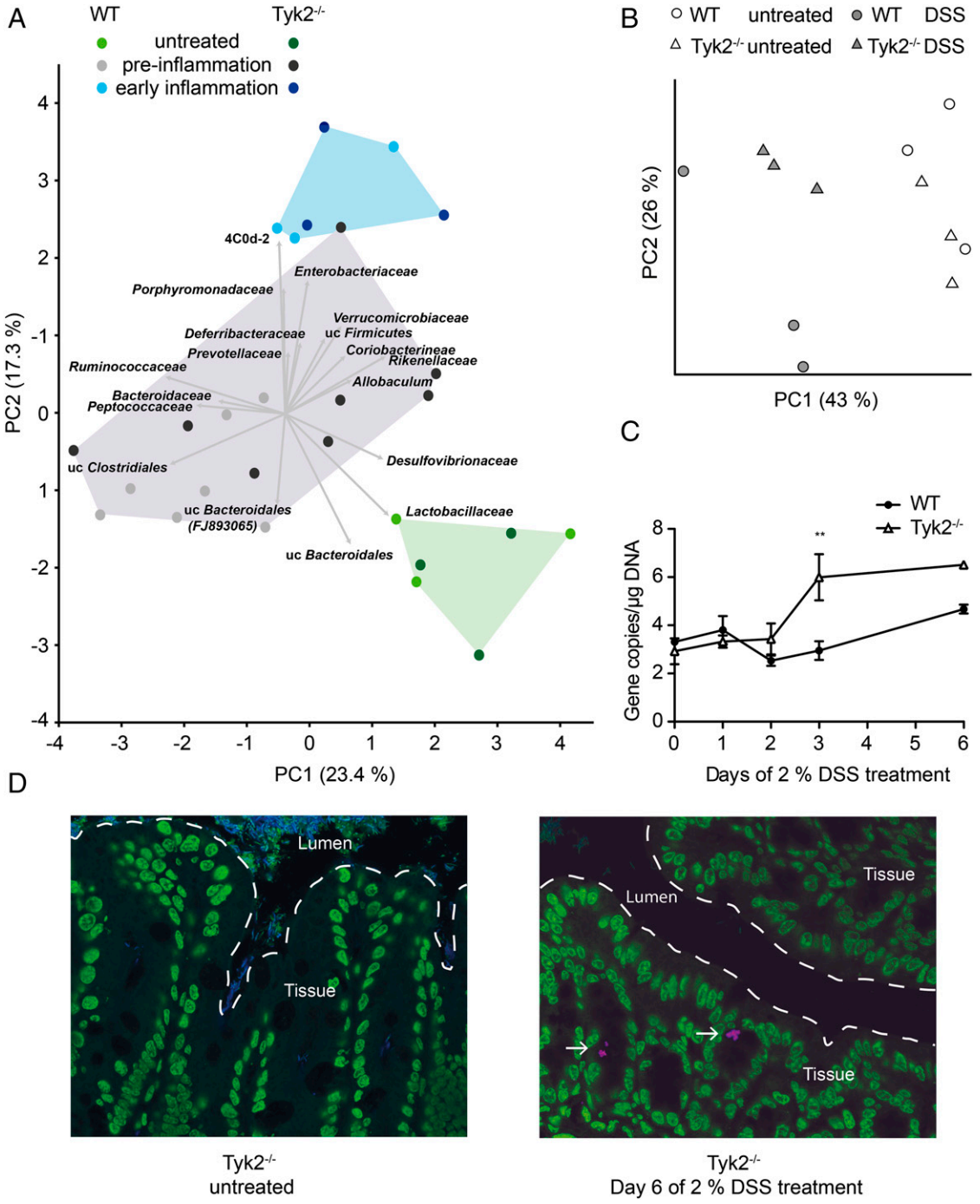

FIGURE 2. DSS and inflammation induce changes in intestinal microbiota composition. (**A**) Principal component analysis (PCA) of taxonomically classified 16S rRNA reads from metatranscriptomes of intestinal microbiota of untreated and DSS-treated WT and *Tyk2*$^{-/-}$ mice. The first two principal components PC1 (*x*-axis) and PC2 (*y*-axis) account for 40.7% of the total variation in the dataset. Three clusters could be observed: 1) untreated (green, day 0), 2) preinflammation DSS-treated (gray, days 1–3), and 3) early DSS-induced inflammation (blue, day 6). Vectors indicate microbial taxa associated with these clusters. Samples from *Tyk2*$^{-/-}$ mice are shown in darker colors. (**B**) Principal coordinate analysis of 16S rRNA gene amplicon libraries from intestinal microbiota of untreated and day 6 DSS-treated WT and *Tyk2*$^{-/-}$ mice based on weighted UniFrac distance. Samples are colored by condition: untreated WT (○) and untreated *Tyk2*$^{-/-}$ (△); DSS-treated WT (●) and DSS-treated *Tyk2*$^{-/-}$ (▲). The 95% confidence limits are smaller than the respective data points (i.e., triangles or circles). Bacterial indicator phylotypes for genotype and treatment are shown in Supplemental Fig. 2B. (**C**) qPCR quantification of *Enterobacteriaceae* 16S rRNA genes (log gene copies per microgram extracted DNA). $^{**}p < 0.01$ for differences between *Enterobacteriaceae* 16S rRNA genes in WT and *Tyk2*$^{-/-}$ mice. (**D**) Fluorescence in situ hybridization image of *Enterobacteriaceae* in untreated and DSS-treated *Tyk2*$^{-/-}$ mice at day 6. Eukaryotic cells are depicted in green (SYBR Green), *Enterobacteriaceae* in pink (Cy3-labeled probe specific for *Enterobacteriaceae*), and other bacteria in blue (Cy5-labeled probe mix targeting all bacteria). Original magnification ×400.

Fluorescence in situ hybridization

A Cy3-labeled oligonucleotide probe specific for the 23S rRNA of *Enterobacteriaceae*, S-*-EBAC-1790-a-A-18 (5′-CGT GTT TGC ACA GTG CTG-3′), was used in combination with an unlabeled competitor probe (5′-CGT GTT TGC AGA GTG CTG-3′) and a Cy5-labeled probe mix targeting all bacteria (EUB 338 I-III) in a 40% formamide hybridization solution under standard hybridization conditions (24). As a eukaryotic stain, SYBR Green was used.

Isolation and stimulation of IECs

Colon and cecum were isolated, cut into 2 to 3 mm pieces, and rinsed in cold PBS. Tissue pieces were then shaken at 37°C in PBS containing 30 mM EDTA for 10 min. The supernatant was centrifuged (1000 × *g*, 5 min) and washed three times in cold PBS and then either frozen in liquid N_2 for RNA or protein isolation or stimulated with rIL-22 (R&D Systems, Minneapolis, MN) at 37°C in RPMI 1640 for 15 min. After stimulation, cells

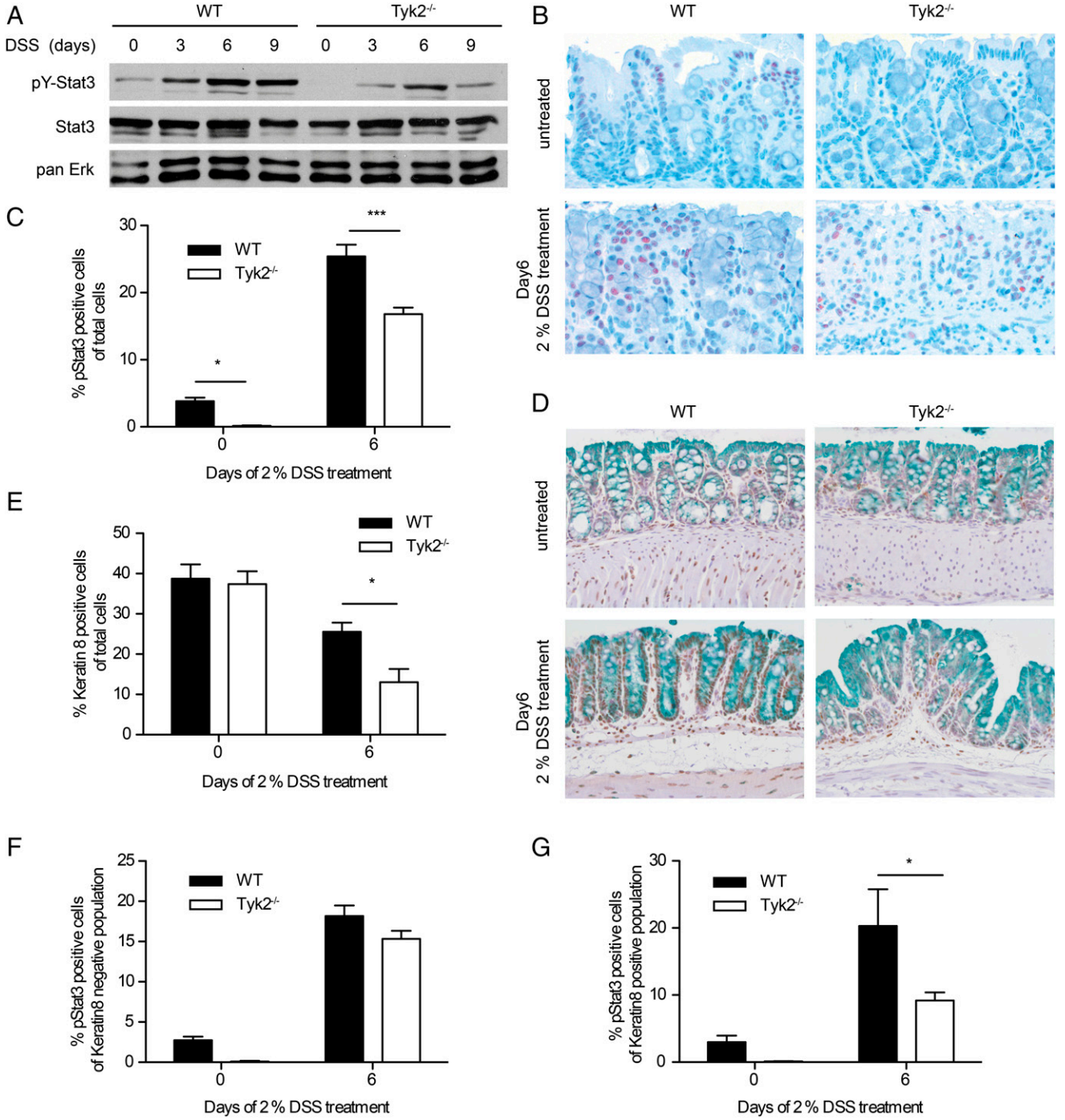

FIGURE 3. Reduced STAT3 phosphorylation in *Tyk2*-deficient colon tissue. (**A**) Western blot for pY-STAT3 on homogenized colon tissue of WT and *Tyk2*$^{-/-}$ mice on days 0, 3, 6, and day 9 of DSS treatment. STAT3 and pan-ERK were used as a loading control. (**B**) Representative images of immunohistochemical staining for pY-STAT3 on day 0 and day 6 of DSS treatment for WT and *Tyk2*$^{-/-}$ mice. Original magnification ×200. (**C**) Quantification of pY-STAT3 immunohistochemistry on WT and *Tyk2*$^{-/-}$ colon tissue sections on days 0 and 6 of DSS treatment using HistoQuest software. Stainings are derived from two independent experiments, with a total of six mice per genotype; a minimum of three images per mouse were quantified. Results are given as mean values ± SEM. (**D**) Representative images of immunohistochemical staining for pY-STAT3 and Keratin8 on day 0 and day 6 of DSS treatment for WT and *Tyk2*$^{-/-}$ mice. Original magnification ×200. (**E–G**) Quantification of immunohistochemistry for Keratin8 and pY-STAT3 using HistoQuest software. Results are derived from two independent experiments with a total of five to six mice per genotype. (E) Keratin8 single-positive cells among total analyzed cells. (F) pY-STAT3^{+} cells among Keratin8^{-} cells. (G) pY-STAT3^{+} cells among Keratin8^{+} cells. *$p < 0.05$, ***$p < 0.001$.

were pelleted and resuspended in RIPA buffer containing 10 mM Tris-HCl (pH 8), 1 mM EDTA, 0.5 mM EGTA, 0.2 mM sodium vanadate, 25 mM sodium fluoride, 140 mM NaCl, 5% glycerol, 0.1% sodium deoxycholate, 0.1% SDS, 1% Triton X-100, 1 mM PMSF, and 1× SigmaFAST protease inhibitor tablet (Sigma-Aldrich) for Western blot analysis.

Western blot analysis

Colon tissue and IEC preparations were homogenized in RIPA buffer (see *Isolation and stimulation of IECs*). Western blots were performed as described previously (25) using the following Abs: rabbit anti–phospho-STAT3 (Tyr^{705}), rabbit anti-STAT3 (both Cell Signaling Technologies, Danvers, MA), mouse anti-panERK (BD Biosciences, San Diego, CA), β-tubulin (Santa Cruz Biotechnology, Dallas, TX), and rabbit anti-RegIIIγ (26) (provided by L. Hooper, University of Texas, Southwestern Medical Center, Dallas, TX).

Immunohistochemistry

Paraffin sections were rehydrated and boiled in a Tris-EDTA–containing buffer (pH 9) for 45 min to unmask Ags, then blocked with 10% goat serum (Zymed, Carlsbad, CA) and incubated with phospho-STAT3 (Tyr^{705}) Ab (Cell Signaling Technologies, Danvers, MA) 1:200 overnight at 4˚C. For double stainings, sections were additionally incubated with Troma 1 rat mAb against cytokeratin-8 (Developmental Studies Hybridoma Bank, Iowa City, IA). To detect proliferation, slides were boiled 20 min in citric buffer (pH 6)

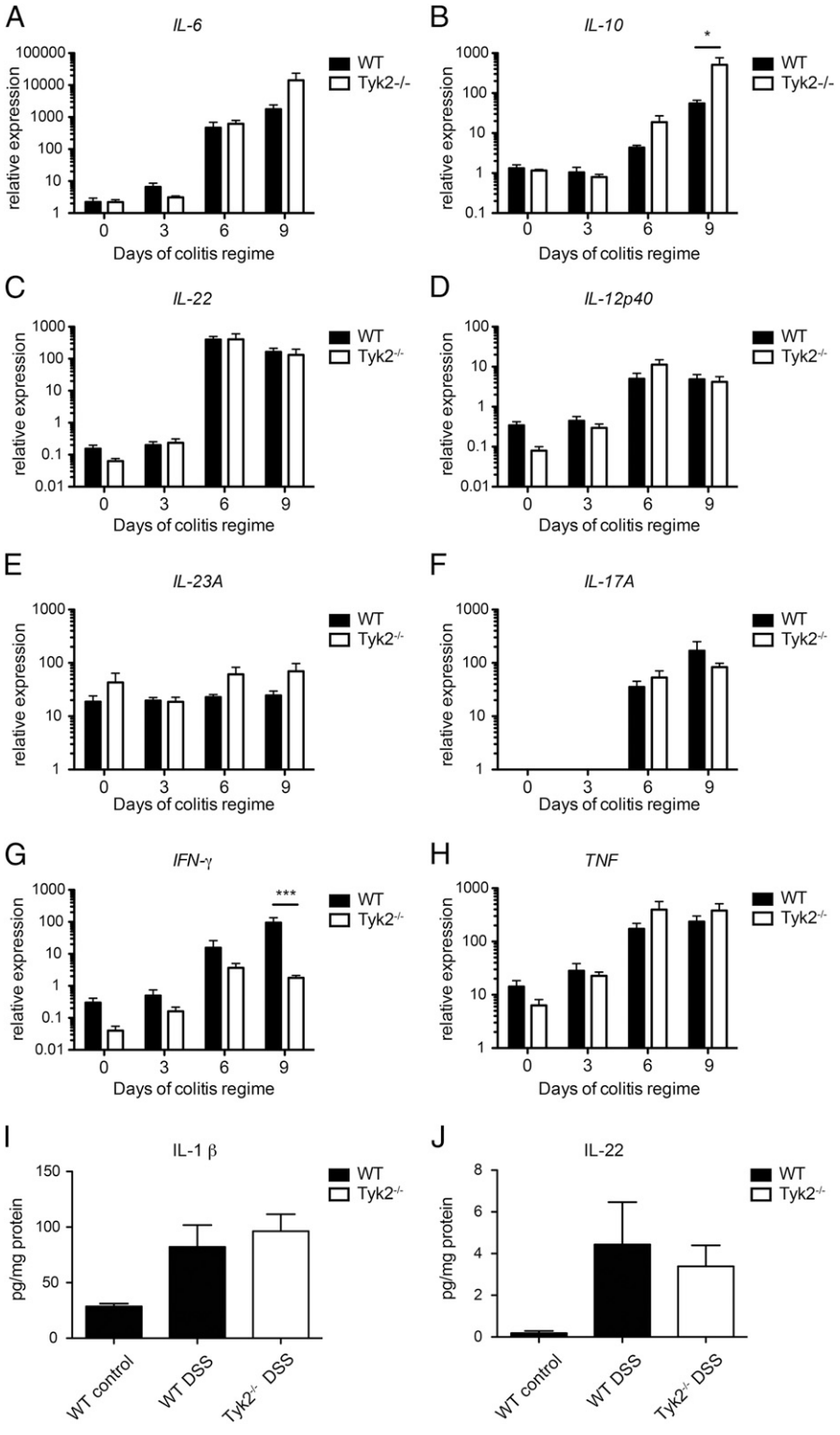

FIGURE 4. Regulation of cytokine expression in *Tyk2*-deficient colons. Real-time qPCR (RT-qPCR) analysis of (**A**–**C**) major STAT3-activating cytokines (IL-6, IL-10, and IL-22, respectively) and (**D**–**H**) other relevant cytokines (IL-12p40, IL-23A, IL-17A, IFN-γ, and TNF, respectively) was performed in colons of WT and $Tyk2^{-/-}$ mice on days 0, 3, 6, and 9 of DSS treatment. Relative expression of target genes was normalized to the endogenous housekeeping gene *Ube2d2*. Data are derived from two independent experiments, each with two to three mice per genotype per treatment. Results are given as mean values ± SEM. $*p < 0.05$, $***p < 0.001$. (**I** and **J**) IL-1β (I) and IL-22 (J) protein levels in healthy and inflamed colon tissue were determined by bead assay ($n = 8$ per genotype and treatment). Results are given as mean values ± SEM.

and incubated with rabbit polyclonal anti-Ki67 (Leica/Novocastra) Ab 1:1000. Sections were then incubated with goat anti-rabbit HRP (Dako) and developed using 3-amino-9-ethylcarbazole substrate kit for single stainings (ID Labs, London, U.K.) or with 3,3′-diaminobenzidine substrate kit (Vector Laboratories, Burlingame, CA) and HistoGreen (Linaris, Dossenheim, Germany) for double stainings. Sections were counterstained with Mayer's hematoxylin and imaged on an epifluorescence microscope (Zeiss Axio Imager), and at least three images per colon were taken. Positive-stained cells were quantified using the HistoQuest software (TissueGnostics, Vienna, Austria) as described previously (10). For determination of goblet cell numbers, deparaffinized formaldehyde-fixed tissue sections were stained with Alcian blue (Sigma-Aldrich). At least five images per colon were taken and mean values of goblet cells per crypt are displayed.

RT-qPCR from colon tissue pieces

RNA was isolated from colon tissue or from isolated IECs using a NucleoSpin RNA II kit (Macherey-Nagel, Düren, Germany) according to the manufacturer's protocol. Real-time qPCR (RT-qPCR) was performed and calculated as described previously (25) unless stated otherwise using the primer sequences or order numbers for Qiagen QuantiTect assays given in Supplemental Table II.

IL-1β and IL-22 determination

Frozen tissue was homogenized in PBS containing proteinase inhibitors (PMSF; Roche cOmplete protease inhibitor mixture), 1 mM vanadate, and 1 mM DTT. The homogenate was freeze-thawed twice. Total protein in the supernatants was determined by bicinchoninic acid assay (Pierce), and IL-1β and IL-22 levels were determined using a FlowCytomix kit (eBioscience) on 25 μl supernatant according to the manufacturer's instructions. The IL-1β and IL-22 amounts were normalized to total protein.

Citrobacter rodentium *infection*

Citrobacter rodentium strain ICC169 (nalidixic acid resistant) was obtained from Siouxsie Wiles (27, 28) and grown in Luria broth (Roth, Karlsruhe, Germany) culture supplemented with nalidixic acid (Sigma-Aldrich) at 37°C. *C. rodentium* ($1–2 \times 10^9$ CFU per mouse) was administered via oral gavage. Control mice received sterile PBS. To determine bacterial load, spleens, ceca, and colons were homogenized on day 7 postinfection and serial dilutions were plated on Luria broth plates supplemented with nalidixic acid. For assessment of intestinal permeability, mice were starved for 4 h on day 7 postinfection and 60 mg/g mouse FITC-dextran (Sigma-Aldrich) was applied via oral gavage. Serum was isolated 5 h later and fluorescence was determined and calculated relative to a standard curve. Serum of untreated mice was used for determination of background levels. For histology, colons were isolated on day 7 postinfection, flushed with PBS (Sigma-Aldrich), and fixed in 7.5% formaldehyde. H&E-stained paraffin sections were imaged and used for pathological evaluation. Sections were scored by a pathologist, and a histological colitis score was assessed for submucosal edema, goblet cell depletion, epithelial hyperplasia, epithelial damage, and neutrophil and mononuclear cell infiltration as described (29, 30).

Statistical analysis

Statistical analysis was performed using GraphPad Prism software (GraphPad Software, San Diego, CA) by one-way ANOVA followed by a Bonferroni post hoc test. For *C. rodentium* infection experiments,

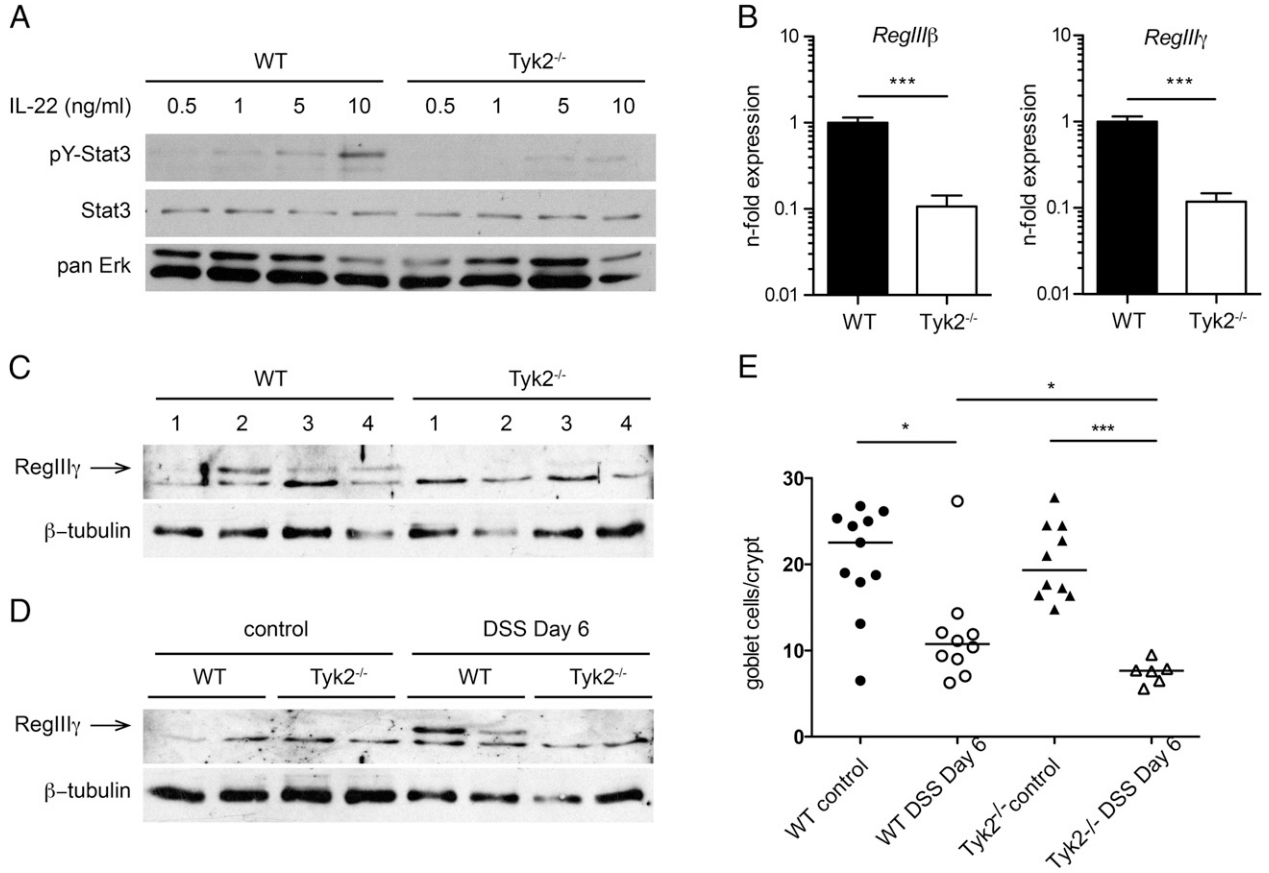

FIGURE 5. Reduced IL-22 signaling and target gene expression in *Tyk2*-deficient mice. (**A**) IECs were isolated from colon tissue of untreated WT and $Tyk2^{-/-}$ mice and stimulated with 0.5, 1, 5, and 10 ng/ml IL-22 for 15 min. Lysates were analyzed for pY-STAT3 on Western blot. STAT3 and pan-ERK were used as a loading control. (**B**) RT-qPCR analysis of IL-22 target genes *RegIIIβ* and *RegIIIγ* in IECs isolated from mice on day 6 of DSS treatment. Relative expression was calculated relative to *Oaz1* and normalized to the respective WT. Data are derived from two independent experiments with a total of 7 mice per genotype. $***p < 0.001$. (**C**) Lysates of IECs isolated from four mice per genotype on day 6 of DSS treatment were analyzed for presence of RegIIIγ by Western blot. β-Tubulin was used as a loading control. (**D**) Colon tissue lysates of untreated and day 6 DSS-treated WT and $Tyk2^{-/-}$ mice were analyzed for RegIIIγ via Western blot. β-Tubulin was used as loading control. (**E**) Quantification of Alcian blue staining of WT and $Tyk2^{-/-}$ colon tissue sections on days 0 and 6 of DSS treatment. Stainings are derived from a total of 6–11 mice per genotype; five images per mouse were quantified. Results are given as mean values ± SEM. $*p < 0.05$, $***p < 0.001$.

statistical analysis was performed using the Mann–Whitney *U* test. A p value <0.05 was considered statistically significant.

Results

Tyk2-deficient mice are highly susceptible to DSS-induced colitis

To characterize the role of *Tyk2* in acute intestinal inflammation, C57BL/6N (WT) and *Tyk2*$^{-/-}$ mice were treated with 2% DSS (w/v) in the drinking water for 7 d and subsequently offered normal water. Weight loss in both genotypes started on average at day 6 of DSS treatment; the experimental endpoint was set at day 9. From day 7 on, *Tyk2*$^{-/-}$ mice lost significantly more weight than did the WT controls (Fig. 1A). Starting on day 3, DSS-treated mice showed intestinal crypt damage and signs of acute inflammation as determined by pathology scoring (Fig. 1B). In accordance with the weight loss, *Tyk2*$^{-/-}$ mice displayed more severe colitis pathology scores compared with WT mice at the experimental endpoint (Fig. 1B). More specifically, almost complete destruction of the epithelium as well as increased infiltration of inflammatory cells was seen in histological sections (Fig. 1C). To further investigate the role of Tyk2 in intestinal inflammation, we employed a second chemically induced model, hapten-induced colitis using TNBS (31). Because C57BL/6 mice are described to be relatively resistant to this model, a presensitization step was included as described (19). WT and *Tyk2*$^{-/-}$ mice were treated intrarectally with 5% TNBS mixed with an equal amount of ethanol on day 0 and where applicable colons were isolated at the indicated time points. In contrast to the DSS model, no major weight loss in both genotypes could be observed (Supplemental Fig. 1A) and no significant differences in colon lengths were detected (Supplemental Fig. 1B). Induction of pathology upon TNBS treatment peaked after 4 d of treatment and recovery already started at day 7 in both WT and *Tyk2*$^{-/-}$ mice (Supplemental Fig. 1C, 1D), indicating that Tyk2 is dispensable for protection against TNBS-induced colitis. We thus focused on the clear effect of Tyk2 in the DSS model in our subsequent analyses.

DSS administration induces characteristic changes in intestinal microbiota structure and activity in WT and Tyk2-deficient mice

Alterations in microbial community composition accompany IBD development in mice and humans and have been observed in DSS-induced colitis models in C57BL/6 mice (21, 24).

To determine the composition and transcriptional activity of the intestinal microbiota in the development of colitis and the absence of *Tyk2*, we performed both bacterial 16S rRNA gene-targeted sequencing and shotgun metatranscriptomics using 454 titanium and Illumina sequencing, respectively. Principal component analysis (PCA) of taxonomically classified 16S rRNA transcripts from the metatranscriptomes revealed that DSS treatment was the major factor driving changes in intestinal microbiota composition (Fig. 2A). The first two principal components PC1 (*x*-axis) and PC2 (*y*-axis) accounted for 40.7% of the total variation in the dataset. Microbial communities clustered into three distinctive groups based on phase of treatment: 1) untreated, 2) preinflammation DSS-treated (on days 1, 2, and 3), and 3) early DSS-induced inflammation (on day 6). The 16S rRNA abundance of several high-level taxa drove the differences in community composition. *Lactobacillaceae* and *Bacteriodales* were characteristic of untreated mice, and several groups such as *Enterobacteriaceae*, *Verrucomicrobiaceae*, *Porphyromonodaceae*, 4C0d-2, and *Deferribacteraceae* were generally characteristic of DSS-induced inflammation, independent from genotype (Fig. 2A and data not shown). Additionally, PCA plots of functionally classified messenger RNAs also revealed treatment phase–dependent clustering of samples (Supplemental Fig. 2). However, only two distinctive groups could be resolved: 1) untreated and 2) DSS treatment. The clustering was driven by contributions from several transcript classes, reflecting a characteristic shift in profiles involving multiple functional categories (e.g., for untreated, sulfur metabolism and respiration; for DSS treatment, protein and RNA metabolism).

During colitis, microbial community composition can experience major shifts at a fine phylogenetic/taxonomic level that are not observed at higher taxonomic levels (21). We therefore also studied changes in the community structure at the more resolved phylotype level using 16S rRNA gene-targeted amplicon pyrosequencing. Microbial community composition shifted significantly between untreated and day 6 DSS-treated mice (Fig. 2B, permutational ANOVA $p = 0.002$). We observed a statistically significant interaction between treatment and genotype ($p = 0.001$), which indicated the presence of a *Tyk2*-specific response of the intestinal microbiota to DSS treatment. Using a statistical model, we identified 39 species-level phylotypes that were significantly associated with DSS-induced inflammation, 34 of which were genotype specific (Supplemental Fig. 2, Supplemental

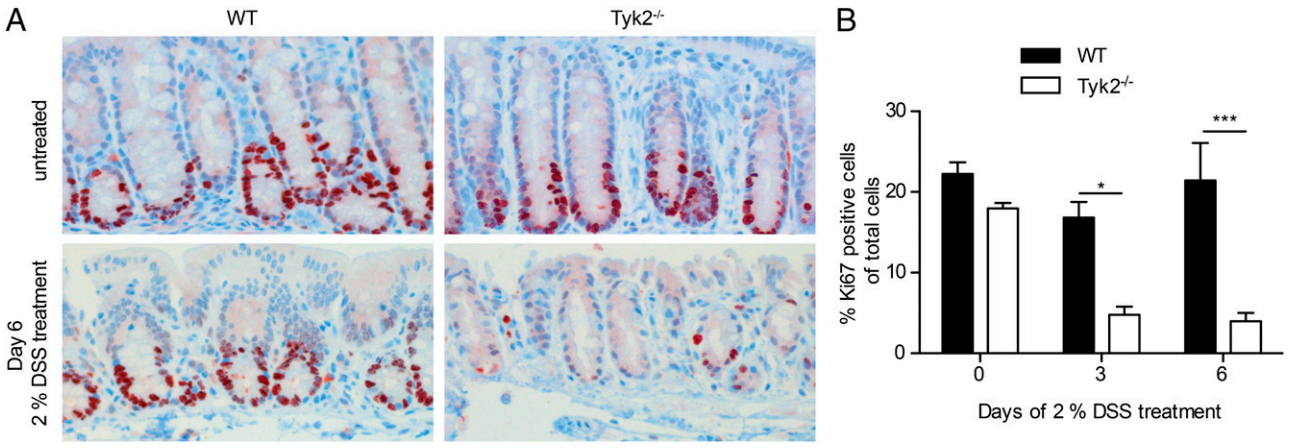

FIGURE 6. Reduced epithelial proliferation in the absence of *Tyk2*. (**A**) Representative images of immunohistochemical staining for Ki67 on colon tissue sections of untreated and day 6 DSS-treated WT and *Tyk2*$^{-/-}$ mice. Original magnification ×200. (**B**) Quantification of Ki67 immunohistochemistry on WT and *Tyk2*$^{-/-}$ colon tissue sections on days 0, 3, and 6 of DSS treatment using HistoQuest software. Stainings are derived from two independent experiments with a total of six mice per genotype; a minimum of three images per mouse were quantified. Results are given as mean values ± SEM. *$p < 0.05$, ***$p < 0.001$.

Table I). For example, one phylotype belonging to *Enterobacteriaceae* was significantly enriched in DSS-treated $Tyk2^{-/-}$ mice and not in WT mice. qPCR using group-specific primers showed an increase in *Enterobacteriaceae* during DSS treatment, with higher enrichment in $Tyk2^{-/-}$ mice at day 3 compared with WT mice (Fig. 2C). Fluorescence in situ hybridization with a group-specific probe also revealed characteristic rod-shaped *Enterobacteriaceae* in the intestinal microbiota of DSS-treated $Tyk2^{-/-}$ mice (Fig. 2D), whereas it was not detectable in WT animals (data not shown) and untreated $Tyk2^{-/-}$ mice. Consistent with this, an increase of mRNA and rRNA transcripts of *Enterobacteriales* was observed in metatranscriptomes of $Tyk2^{-/-}$ mice (data not shown).

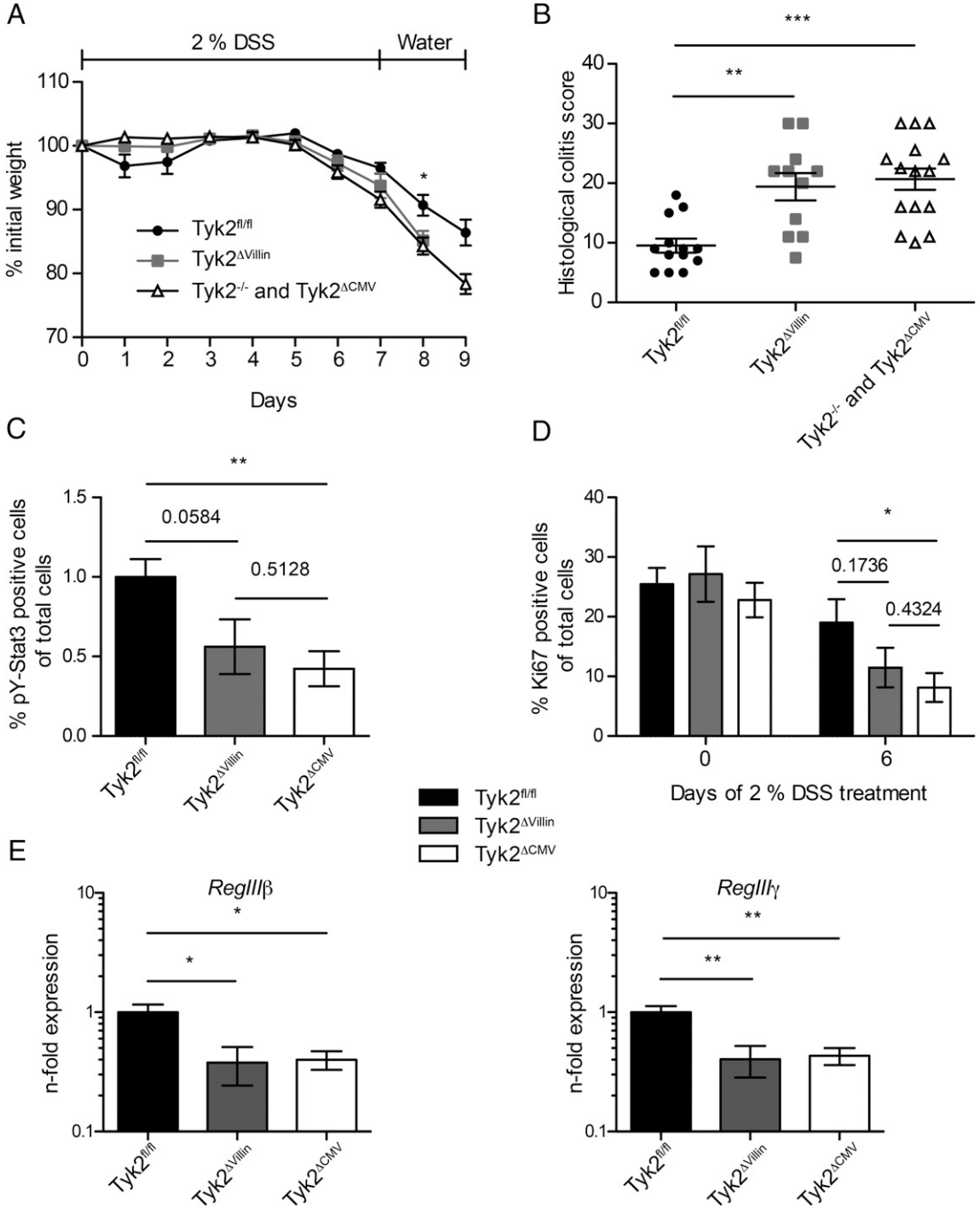

FIGURE 7. Tyk2 in IECs crucially contributes to protection against acute colitis. (**A** and **B**) $Tyk2^{fl/fl}$, $Tyk2^{\Delta Villin}$, and $Tyk2^{-/-}$ or $Tyk2^{\Delta CMV}$ littermate mice were treated with 2% DSS for 7 d, followed by 2 d of water. Data are derived from three independent experiments each with three to five mice per genotype per treatment. (A) Weight loss was determined daily and is displayed relative to initial weight. Results are given as mean values ± SEM. (B) Histological scores are shown for day 9 of colitis regimen. Results for individual mice and mean values are depicted. (**C** and **D**) Quantification of immunohistochemistry for pY-STAT3 (C) or Ki67 (D) of $Tyk2^{fl/fl}$, $Tyk2^{\Delta Villin}$, and $Tyk2^{\Delta CMV}$ colon tissue sections on days 0 and 6 of DSS treatment using HistoQuest software. Data are derived from two independent experiments with a total of six mice per genotype per treatment; a minimum of three images per mouse were quantified. (**E**) Expression of *RegIIIβ* and *RegIIIγ* mRNA in IECs isolated from untreated $Tyk2^{fl/fl}$, $Tyk2^{\Delta Villin}$, and $Tyk2^{\Delta CMV}$ mice was determined by RT-qPCR. Relative expression was calculated relative to *Oaz1* and normalized to $Tyk2^{fl/fl}$. Data are derived from two independent experiments with a total of six mice per genotype. Results are given as mean values ± SEM. $*p < 0.05$, $**p < 0.01$, $***p < 0.001$.

Colitis-induced STAT3 tyrosine phosphorylation is reduced in Tyk2-deficient IECs

STAT3 activity is associated with colitogenic as well as anti-inflammatory cytokines such as IL-6, IL-10, IL-12, IL-22, IL-23, and type I IFNs (8, 32). Activation of STAT3 by these cytokines has been reported to be, at least partially, dependent on Tyk2 (1). Thus, we investigated tyrosine phosphorylation of STAT3 (pY-STAT3) by Western blot of whole colonic tissue extracts of WT and *Tyk2*$^{-/-}$ mice in the course of colitis. In healthy animals pY-STAT3 was low in WT and not detectable in *Tyk2*$^{-/-}$ mice. pY-STAT3 increased in both genotypes with a peak on day 6 of DSS treatment; however, levels were markedly decreased in *Tyk2*-deficient animals (Fig. 3A).

Because the contribution of STAT3 to colitis varies depending on the cell type activating STAT3 (32), we determined the major sites of pY-STAT3 by immunohistochemistry. As expected from Western blot analysis, few pY-STAT3^{+} cells were found in untreated mice (Fig. 3B, *upper panels*), whereas on day 6 of DSS treatment a large number of cells contained pY-STAT3 in WT mucosa and fewer cells were positive in *Tyk2*-deficient mucosa (Fig. 3B, *lower panels*). Quantification of pY-STAT3^{+} cells confirmed the highly significant reduction of pY-STAT3 in *Tyk2*-deficient mice (Fig. 3C). The overall numbers of Keratin8^{+} (i.e., epithelial) cells were similar in untreated WT and *Tyk2*$^{-/-}$ mice. DSS treatment led to greater loss of Keratin8^{+} cells in *Tyk2*$^{-/-}$ mice (Fig. 3D, 3E), consistent with the more severe pathology at day 9 (Fig. 1B). WT and *Tyk2*$^{-/-}$ mice had slightly decreased numbers of nonepithelial cells (Keratin8^{-}) with activated STAT3 (Fig. 3D, 3F), whereas pY-STAT3^{+}/Keratin8^{+} cells were significantly decreased in *Tyk2*$^{-/-}$ colonic tissue (Fig. 3D, 3G).

Tyk2 does not affect the expression of most colitis-associated cytokines

To further characterize the mechanism underlying the reduced pY-STAT3 in *Tyk2*$^{-/-}$ IECs, we measured mRNA expression profiles of relevant cytokines in colonic tissues (8). IL-6, IL-10, and IL-22 are the most likely candidate cytokines involved in the IEC-specific activation of STAT3 in a Tyk2-dependent manner (1, 32). Colonic tissue reacted to DSS treatment with an increased *IL-6*, *IL-10*, and *IL-22* mRNA expression from days 3 to 6 on with no significant differences between WT and *Tyk2*$^{-/-}$ animals except for elevated *IL-10* mRNA levels on day 9 (Fig. 4A–C). IL-22 production was further verified on protein level also showing no significant differences between WT and *Tyk2*$^{-/-}$ tissue upon DSS treatment (Fig. 4J).

Tyk2 was shown to impact on IL-12 and IL-23 production and on IL-12–dependent *IFN-γ* as well as IL-23–dependent *IL-17* mRNA expression by various immune cells (1). Colitis-induced increase of *IL-12p40*, *IFN-γ*, and *IL-17A* transcription was observed in both genotypes whereas expression of *IL-23A* remained grossly unaltered (Fig. 4D–G). A significant genotype-related difference could be detected for *IFN-γ* expression on day 9 (Fig. 4G).

TNF and IL-1 β are also central in colitis (8). TNF was transcriptionally activated starting at days 3–6 of DSS regimen without significant variation between WT and *Tyk2*$^{-/-}$ colons (Fig. 4H). Similarly, production of IL-1 β was not altered between WT and *Tyk2*$^{-/-}$ colons (Fig. 4I).

Taken together, alterations in the production of STAT3-inducing, Th1/Th17 axis, or proinflammatory cytokines do not seem to be the major cause for the phenotype observed in *Tyk2*$^{-/-}$ mice, because most cytokines follow a similar expression pattern in WT and mutant mice. Reduced *IFN-γ*, which was expected due to the well-described function of Tyk2 in cytokine-mediated IFN-γ production (1), and enhanced *IL-10* expression, which might be induced as a consequence of an overall increased inflammation in *Tyk2*$^{-/-}$ colon tissue at later time points, resemble an anti-inflammatory condition. However, this is not likely to cause the observed pathology, because both conditions reach significance only at late stages and are expected to protect mice from DSS-induced inflammation (33, 34).

IL-22 signaling and target gene expression are compromised in Tyk2-deficient IECs

Next we evaluated the influence of *Tyk2* deletion on cytokine responsiveness in IECs and in colitis. IL-22 is the major STAT3-activating cytokine in IECs in DSS-induced colitis (35). Isolated primary murine IECs showed a basal level of pY-STAT3 and a dose-dependent increase upon treatment with IL-22 (Fig. 5A). In *Tyk2*$^{-/-}$ IECs, this response was drastically reduced (Fig. 5A). To test the relevance of the impaired IL-22 signaling in vivo, we analyzed the expression of *RegIIIβ* and *RegIIIγ*, which at present are known targets of IL-22 signaling in IECs (35, 36). IECs were isolated from DSS-treated mice and levels of *RegIIIβ* and *RegIIIγ* mRNA were measured by RT-qPCR. Expression of both IL-22 response genes was significantly reduced in *Tyk2*-deficient animals (Fig. 5B). This result was confirmed on the protein level using Western blot analysis of IEC preparations derived from four different mice per genotype, where RegIIIγ was hardly detectable in *Tyk2*$^{-/-}$ IECs compared with WT IECs (Fig. 5C). In untreated colon tissue homogenates, RegIIIγ protein was undetectable in both genotypes; however, the protein could be detected on day 6 of DSS colitis in WT colons whereas it was again absent in *Tyk2*-deficient colons (Fig. 5D). As IL-22 is also involved in goblet cell protection during colitis (37), we furthermore analyzed the number of goblet cells after DSS treatment using Alcian blue staining. As described (38), DSS treatment results in a depletion of goblet cells, which is modestly but significantly more pronounced in the absence of Tyk2 (Fig. 5E).

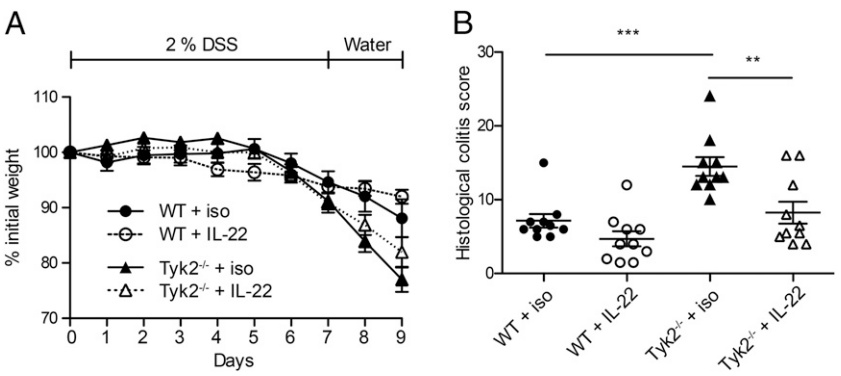

FIGURE 8. *Tyk2* deficiency can be overcome by excess IL-22–Fc in murine DSS colitis. (**A** and **B**) WT and *Tyk2*$^{-/-}$ mice were treated with 2% DSS for 7 d, followed by 2 d of water. Where indicated, mice were treated with 50 μg mIL-22–Fc or isotype control Ab every 3 d. (A) Weight loss was measured daily and is displayed relative to initial weight. Data depicted are derived from one representative experiment with five mice per genotype. Results are given as mean ± SEM. (B) Histological scores are shown for day 9 of DSS treatment. Data are derived from two independent experiments with five mice per genotype per experiment. $^{**}p < 0.01$, $^{***}p < 0.001$.

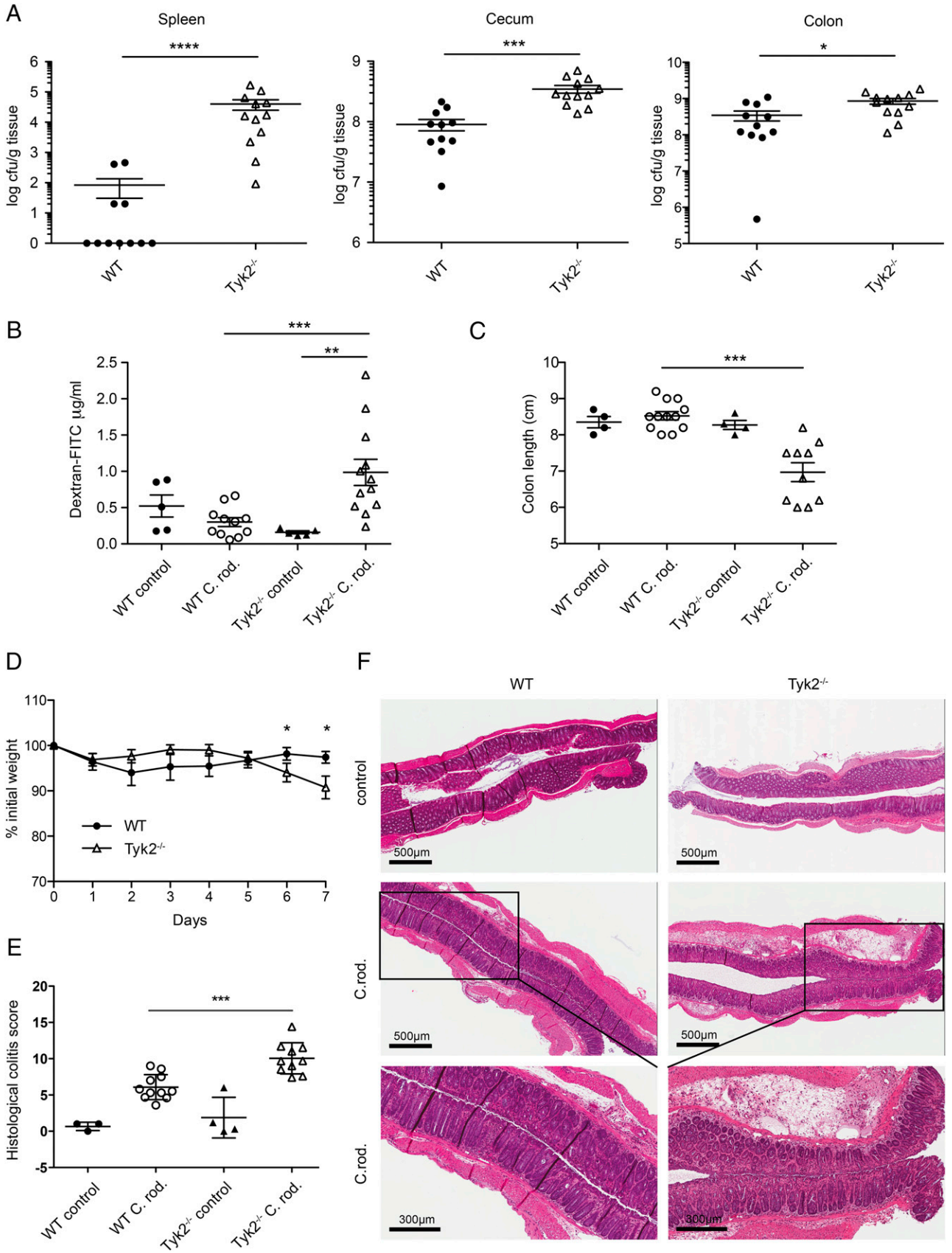

FIGURE 9. *Tyk2* deficiency leads to susceptibility to *C. rodentium* infection. (**A**–**F**) WT and *Tyk2*$^{-/-}$ mice were infected orally with 1–2 × 10^9 CFU *C. rodentium* for 7 d. (A) Translocation of bacteria to the spleen (*left panel*) as well as bacterial load in cecum (*middle panel*) and colon (*right panel*) was determined and is displayed as log CFU/g tissue. Data depicted are from two independent experiments with five to six mice per genotype. (B) Intestinal permeability was measured by determining the concentration of FITC-dextran in the serum. Data depicted are from two independent experiments with five to six mice per genotype. (C) Colon length was determined on day 7 postinfection. (A–C) Results for individual mice and mean values are depicted. (D) Weight loss was determined daily and is displayed relative to initial weight. Data are derived from two independent experiments (*Figure legend continues*)

Reduced epithelial proliferation in the absence of Tyk2

IL-22 signaling via STAT3 in IECs has an important role in mucosal wound healing and promotes epithelial proliferation (35). Proliferating cells of the colon were determined in WT and *Tyk2*-deficient mice using histological staining for Ki67 (39). Untreated mice showed comparable staining for $Ki67^+$ cells (Fig. 6A, *upper panel*). In WT, the number of $Ki67^+$ cells did not significantly change during early colitis. However, in *Tyk2*-deficient colon tissue on days 3 and 6 of DSS treatment, proliferating cells were significantly reduced (Fig. 6).

Tyk2 in IECs crucially contributes to the protection against acute colitis

To evaluate whether the defective IL-22/STAT3 response in $Tyk2^{-/-}$ mice is an epithelial cell–intrinsic effect, we crossed mice carrying floxed alleles of *Tyk2* ($Tyk2^{fl/fl}$) that were recently generated in our laboratory (15) to a mouse line expressing Cre recombinase under the control of the *Villin* promoter (16). In the resulting $Tyk2^{\Delta Villin}$ mice, RT-qPCR in isolated IECs demonstrated that Cre-mediated Tyk2 depletion was highly efficient (data not shown). $Tyk2^{fl/fl}$ mice crossed to a CMV-Cre line ($Tyk2^{\Delta CMV}$) served as the corresponding complete *Tyk2*-deficient control and displayed similar colitis development as did conventional $Tyk2^{-/-}$ mice (data not shown). The weight curves of $Tyk2^{\Delta Villin}$ and $Tyk2^{\Delta CMV}$ (or $Tyk2^{-/-}$) mice after DSS treatment were similar and showed more weight loss compared with $Tyk2^{fl/fl}$ (WT) littermate controls (Fig. 7A). IEC-specific depletion of Tyk2 led to pathohistological colitis scores similar to $Tyk2^{-/-}$ mice (Fig. 7B). As observed for $Tyk2^{-/-}$, $Tyk2^{\Delta CMV}$ mice displayed reduced pY-STAT3 levels in colon tissue, whereas $Tyk2^{\Delta Villin}$ mice showed an intermediate phenotype (Fig. 7C). Proliferation of cells was reduced in the colons of $Tyk2^{\Delta Villin}$ mice, albeit differences to $Tyk2^{fl/fl}$ and $Tyk2^{\Delta CMV}$ did not reach statistical significance (Fig. 7D). However, consistent with the data obtained above, expression of *RegIIIβ* and *RegIIIγ* was similarly diminished in $Tyk2^{\Delta Villin}$ and $Tyk2^{\Delta CMV}$ IEC fractions (Fig. 7E). Collectively, we demonstrate an epithelial cell–intrinsic role for Tyk2 during DSS-induced colitis.

$Tyk2^{-/-}$ mice are rescued by rIL-22Fc from the development of severe colitis

Depletion of murine Tyk2 leads to partial impairment of the cytokine signals transduced from the cognate receptors (1). In line with the published observations, we detected pY-STAT3 in $Tyk2^{-/-}$ IECs upon treatment with high IL-22 doses (Fig. 5A). This led us to the hypothesis that in vivo Tyk2 deficiency can be bypassed by administration of exogenous IL-22. We used an mIL-22Fc fusion protein and followed a protocol resulting in therapeutic effects of IL-22 in colitis models (20, 36). DSS-induced colitis in $Tyk2^{-/-}$ mice was ameliorated to WT levels by excess administration of IL-22Fc, whereas in WT mice no significant improvement of weight loss and colitis scores was observed (Fig. 8).

$Tyk2^{-/-}$ mice are prone to IL-22–dependent bacterial colitis

Intact IL-22 signaling is critical for the host defense against colitis induced by *C. rodentium* (*Enterobacteriaceae*) (40). Therefore, we infected WT and *Tyk2*-deficient mice with this intestinal pathogen to confirm the role of *Tyk2* in an IL-22–dependent colitis model. *Tyk2*-deficient animals show a significantly higher bacterial load in cecum and colon and severely impaired invasion resistance against *C. rodentium* as monitored by splenic bacterial load (Fig. 9A). Increased bacterial load was accompanied by impaired barrier integrity (Fig. 9B), decreased colon length (Fig. 9C), and increased weight loss (Fig. 9D) of *Tyk2*-deficient mice in response to *C. rodentium* infection. Accordingly, $Tyk2^{-/-}$ mice displayed more severe colitis pathology scores compared with WT mice (Fig. 9E) and more severe inflammation (Fig. 9E, 9F).

Taken together, our results clearly demonstrate a critical role of epithelial Tyk2 in protection during both DSS and bacteria-mediated colitis.

Discussion

The protective functions of the protein tyrosine kinase Tyk2 are mainly linked to cytokine responses involved in immunity to infection and cancer (1, 7). Genome-wide association studies identified *Tyk2* as susceptibility locus for IBD in humans (41). During inflammation, $Tyk2^{-/-}$ mice show opposing phenotypes in that they are either protected from Th1- or Th17-driven diseases (4, 5, 42, 43) or more prone to Th2- or Th9-dominated pathology (2, 3). To our knowledge, we are the first to show that murine Tyk2 protects against acute colitis induced either by chemical irritation or by bacterial infection (Figs. 1, 9). Loss of IL-22 and IEC STAT3 leads to more severe acute colitis (35, 44, 45). In the present study, we place the IEC-specific Tyk2 as a crucial protective effector downstream of the IL-22R and as an upstream kinase of STAT3. Using three mouse colitic models, our data suggest that the underlying pathomechanism in the absence of Tyk2 is rather a perturbance of the intestinal epithelial barrier involving insufficient expression of antimicrobial peptides as well as impairment in epithelial regeneration during inflammation than an imbalance of Th cell polarization.

A previous study using *Tyk2*-deficient mice has identified the kinase as an important constituent of the Th1/Th17 axes in DSS-induced colitis and hence a promoter of the disease (42). In contrast to this study, we did not detect a significant influence of *Tyk2* deletion on levels of *IL-12p40* and *IL-23A* mRNA. Furthermore, *IL-17A* or *IL-22* mRNA levels were also not altered (Fig. 4). The discrepancy to our findings may be explained by the differing susceptibility of C57BL/6 (this study) and BALB/c strains to DSS-induced colitis (46) and/or the strain- and housing-dependent differences in the microbiota (47). Additionally, different DSS concentrations (2% in the present study versus 3%) were used, which may lead to opposing effects in the outcome of colitis pathology as we described recently (10). In the TNBS model, which is a mainly Th1-driven model of acute colitis (31, 48), Tyk2 is not essential to protect against colitis (Supplemental Fig. 1). Interestingly, EtOH-treated $Tyk2^{-/-}$ control mice reacted with a significantly increased pathology score caused by the mild disturbance of the epithelial barrier compared with EtOH-treated WT mice, which remained unaffected (Supplemental Fig. 1C). These results further support a cell type–specific function of Tyk2 in the protection against acute colitis with a strongly protective role in epithelial cells but a negligible (this study) or detrimental role (40) in T cells.

Acute colitis induced significantly lower pY-STAT3 in $Tyk2^{-/-}$ colonic tissue, and this could be grossly confined to IECs (Fig. 3). Previous reports demonstrated a requirement of Tyk2 for full-fledged STAT3 activation upon inflammation for lymphoid tissues (4) and keratinocytes (5). As expected (8), the expression of

with six mice per genotype. Results are given as mean values ± SEM. (E) Histological scores for day 7 postinfection. Results for individual mice and mean values ± SEM are depicted. (F) WT and $Tyk2^{-/-}$ colon tissue sections were stained with H&E. Representative images are shown for untreated mice and for mice on day 7 postinfection. *$p < 0.05$, **$p < 0.01$, ***$p < 0.001$, ****$p < 0.0001$.

the major STAT3-activating cytokines IL-6 and IL-22 was elevated during colitis, albeit with no genotype differences that could account for the impaired pY-STAT3 in *Tyk2*$^{-/-}$ mice (Fig. 4). Tyk2 is dispensable for IL-6–mediated signaling in mice (1). Instead, IL-22R signaling was impaired in the absence of Tyk2 and responsible for the diminished pY-STAT3 in IECs (Fig. 5). A biologically significant contribution of Tyk2 to IL-22R signaling has also been found in murine keratinocytes (5) and hepatocytes (49).

The antimicrobial proteins RegIIIβ and RegIIIγ are protective during colitis and have been previously described as direct targets of IL-22/STAT3 in colonic epithelial cells (35, 40, 50). Consistent with impaired STAT3 activation upon IL-22 stimulation in *Tyk2*$^{-/-}$ IECs, RegIII mRNA and protein induction was strongly reduced in IECs and colon tissue isolated from inflamed *Tyk2*$^{-/-}$ mice (Fig. 5). Goblet cell depletion is a characteristic feature of IBD (38). In line with the described protection of goblet cells by IL-22 (37), we found more severe goblet cell depletion in *Tyk2*$^{-/-}$ mice upon DSS treatment (Fig. 5). Consistent with the pivotal function of STAT3 in maintaining or restoring the IEC integrity in homeostasis or colitis (35, 51), we furthermore found a severe proliferation defect in *Tyk2*$^{-/-}$ colonic epithelial cells (Fig. 6).

The central role of epithelial-specific Tyk2 is demonstrated by the use of conditional *Tyk2*$^{\Delta Villin}$ mice, which recapitulated the phenotype observed in complete *Tyk2*-deficient mice with respect to histopathological colitis score and IL-22/STAT3 target gene expression (Fig. 7). However, the proliferation defect and the decreased level of STAT3 activation in colonic tissue of *Tyk2*$^{\Delta Villin}$ mice appeared less severe as in *Tyk2*$^{-/-}$ mice. This indicates the expected function of Tyk2 in cells other than IECs and through other cytokines than IL-22. Likely candidates are IFN-I, IL-23, and IL-27, which engage Tyk2 for production and/or signaling and have been shown to counteract acute DSS colitis (10, 36, 52).

The IL-22R is composed of IL-10R2 and IL-22R1 and in addition to Tyk2 engages Jak1 for signal transduction (53). Consistent with observations by others (5, 49) we report residual IL-22 responsiveness in the absence of Tyk2 (Fig. 5). In agreement with these findings we show that excess exogenous IL-22 ameliorates DSS-induced colitis in *Tyk2*$^{-/-}$ mice (Fig. 8). Our findings underscore the potential of rIL-22 to restore inflammation-damaged intestinal epithelia (20, 36, 54). Albeit not proven formally, a likely mechanistic explanation is the promotion of IL-22/STAT3–mediated epithelial barrier integrity through residual IL-22R signaling at high dose in the absence of Tyk2.

Infection with *C. rodentium* results in induction of acute colitis critically depending on the IL-22/STAT3 axis (55, 56). Absence of Tyk2 leads to a significantly increased bacterial load in spleen, cecum, and colon (Fig. 9), with the strongest effect observed in the spleen. This result and the significantly increased permeability to a fluorescent tracer point to an important role of Tyk2 in maintaining epithelial barrier integrity in response to bacterial-induced colitis. Consequently, *Tyk2*-deficient mice display also more severe pathology compared with WT mice (Fig. 9). These results complement our findings on the crucial role of Tyk2 in IL-22–mediated colitis protection.

The interdependence of the host and the gut microbiome under homeostatic and inflammatory conditions is well established (13, 57). We confirmed that the intestinal microbiota composition and activity were dramatically shifted upon DSS treatment (10, 21, 24). The community structure of *Tyk2*-deficient mice upon administration of DSS had shifts distinctive from diseased WT mice, including generally elevated levels of *Enterobacteriaceae*, which have been associated with colitis (21, 58, 59), and differences in specific species-level phylotypes (Fig. 2). Interestingly, mice deficient for IL-22 have altered microbiota composition compared with WT mice (60) and show decreased susceptibility to pathogenic *Salmonella* due to overgrowth of commensals such as *Enterobacteriaceae* (61). However, further studies are necessary to determine the exact influence of the IL-22/Tyk2 signaling pathway on structuring the intestinal microbiota composition and activity. Our results support the link between *Enterobacteriaceae* abundance and inflammation severity in the DSS model (10, 21) and that relative abundance of intestinal *Enterobacteriaceae* could serve as a predictive marker of acute colitic flares. Additionally, in the present study *Enterobacteriaceae* were identified not only in the gut lumen but also within the underlying mucosal tissue (Fig. 2D), indicating that members of this group might provoke inflammation.

We suggest that depending on the severity of inflammatory stimuli, the chronicity, and the genetic factors, Tyk2 is either anticolitogenic by promoting mucosal healing through IL-22/STAT3 action in IECs or colitogenic by elevating the Th1 and Th17 adaptive immune responses. By analogy, it was also observed for IL-22 and STAT3 that in addition to the protective IEC-restricted function in colitis, pathogenic effects may occur through perturbation of cytokine levels and/or immune cell recruitment/activation (62, 63). The complex Tyk2 functions in mice are also reflected in humans, because variation occurs between human populations with respect to Crohn's disease susceptibility and its correlation to the Tyk2 and STAT3 loci (64). In conclusion, a future use of Tyk2 inhibitors (65, 66) for the treatment of colitis should carefully consider whether the primary therapeutic benefit is expected through the regeneration of the epithelial barrier or the dampening of the hyperinflammation.

Acknowledgments

We thank Claus Vogl for statistical support; Graham Tebb for critical reading of the manuscript; Ursula Reichart for microscopy and support in mouse breeding; Barbara Wallner for support in mouse breeding; and Doris Rigler, Carolin Hamann, Bettina Tutzer, Marion Bokor, and Natalija Bozovic for technical assistance. We are grateful to Ingrid Walter and Melanie Korb (Vetcore, University of Veterinary Medicine, Vienna) for excellent technical help with histology. We also thank Siouxsie Wiles (University of Auckland, Auckland, New Zealand) for providing *C. rodentium* ICC169, Lora Hooper (University of Texas, Southwestern Medical Center, Dallas, TX) for providing anti-RegIIIγ Ab, and Genentech (South San Francisco, CA) for mIL-22Fc.

Disclosures

The authors have no financial conflicts of interest.

References

1. Strobl, B., D. Stoiber, V. Sexl, and M. Mueller. 2011. Tyrosine kinase 2 (TYK2) in cytokine signalling and host immunity. *Front. Biosci. (Landmark Ed.)* 16: 3214–3232.
2. Seto, Y., H. Nakajima, A. Suto, K. Shimoda, Y. Saito, K. I. Nakayama, and I. Iwamoto. 2003. Enhanced Th2 cell-mediated allergic inflammation in Tyk2-deficient mice. *J. Immunol.* 170: 1077–1083.
3. Übel, C., A. Graser, S. Koch, R. J. Rieker, H. A. Lehr, M. Müller, and S. Finotto. 2014. Role of Tyk-2 in Th9 and Th17 cells in allergic asthma. *Sci. Rep.* 4: 5865.
4. Ishizaki, M., R. Muromoto, T. Akimoto, Y. Ohshiro, M. Takahashi, Y. Sekine, H. Maeda, K. Shimoda, K. Oritani, and T. Matsuda. 2011. Tyk2 deficiency protects joints against destruction in anti-type II collagen antibody-induced arthritis in mice. *Int. Immunol.* 23: 575–582.
5. Ishizaki, M., R. Muromoto, T. Akimoto, Y. Sekine, S. Kon, M. Diwan, H. Maeda, S. Togi, K. Shimoda, K. Oritani, and T. Matsuda. 2014. Tyk2 is a therapeutic target for psoriasis-like skin inflammation. *Int. Immunol.* 26: 257–267.
6. Kilic, S. S., M. Hacimustafaoglu, S. Boisson-Dupuis, A. Y. Kreins, A. V. Grant, L. Abel, and J. L. Casanova. 2012. A patient with tyrosine kinase 2 deficiency without hyper-IgE syndrome. *J. Pediatr.* 160: 1055–1057.
7. Minegishi, Y., M. Saito, T. Morio, K. Watanabe, K. Agematsu, S. Tsuchiya, H. Takada, T. Hara, N. Kawamura, T. Ariga, et al. 2006. Human tyrosine kinase 2 deficiency reveals its requisite roles in multiple cytokine signals involved in innate and acquired immunity. *Immunity* 25: 745–755.
8. Neurath, M. F. 2014. Cytokines in inflammatory bowel disease. *Nat. Rev. Immunol.* 14: 329–342.

9. Coskun, M., M. Salem, J. Pedersen, and O. H. Nielsen. 2013. Involvement of JAK/STAT signaling in the pathogenesis of inflammatory bowel disease. *Pharmacol. Res.* 76: 1–8.
10. Rauch, I., E. Hainzl, F. Rosebrock, S. Heider, C. Schwab, D. Berry, D. Stoiber, M. Wagner, C. Schleper, A. Loy, et al. 2014. Type I interferons have opposing effects during the emergence and recovery phases of colitis. *Eur. J. Immunol.* 44: 2749–2760.
11. Rauch, I., F. Rosebrock, E. Hainzl, S. Heider, A. Majoros, S. Wienerroither, B. Strobl, S. Stockinger, L. Kenner, M. Müller, and T. Decker. 2015. Noncanonical effects of IRF9 in intestinal inflammation: more than type I and type III interferons. *Mol. Cell. Biol.* 35: 2332–2343.
12. Rauch, I., M. Müller, and T. Decker. 2013. The regulation of inflammation by interferons and their STATs. *JAK-STAT* 2: e23820.
13. Kamada, N., S. U. Seo, G. Y. Chen, and G. Núñez. 2013. Role of the gut microbiota in immunity and inflammatory disease. *Nat. Rev. Immunol.* 13: 321–335.
14. Maloy, K. J., and F. Powrie. 2011. Intestinal homeostasis and its breakdown in inflammatory bowel disease. *Nature* 474: 298–306.
15. Vielnascher, R. M., E. Hainzl, N. R. Leitner, M. Rammerstorfer, D. Popp, A. Witalisz, R. Rom, M. Karaghiosoff, T. Kolbe, S. Müller, et al. 2014. Conditional ablation of TYK2 in immunity to viral infection and tumor surveillance. *Transgenic Res.* 23: 519–529.
16. El Marjou, F., K. P. Janssen, B. H. Chang, M. Li, V. Hindie, L. Chan, D. Louvard, P. Chambon, D. Metzger, and S. Robine. 2004. Tissue-specific and inducible Cre-mediated recombination in the gut epithelium. *Genesis* 39: 186–193.
17. Teppner, I., B. Aigner, E. Schreiner, M. Müller, and M. Windisch. 2004. Polymorphic microsatellite markers in the outbred CFW and ICR stocks for the generation of speed congenic mice on C57BL/6 background. *Lab. Anim.* 38: 406–412.
18. Mähler Convenor, M., M. Berard, R. Feinstein, A. Gallagher, B. Illgen-Wilcke, K. Pritchett-Corning, and M. Raspa, FELASA working group on revision of guidelines for health monitoring of rodents and rabbits. 2014. FELASA recommendations for the health monitoring of mouse, rat, hamster, guinea pig and rabbit colonies in breeding and experimental units. *Lab. Anim.* 48: 178–192.
19. Wirtz, S., C. Neufert, B. Weigmann, and M. F. Neurath. 2007. Chemically induced mouse models of intestinal inflammation. *Nat. Protoc.* 2: 541–546.
20. Ota, N., K. Wong, P. A. Valdez, Y. Zheng, N. K. Crellin, L. Diehl, and W. Ouyang. 2011. IL-22 bridges the lymphotoxin pathway with the maintenance of colonic lymphoid structures during infection with *Citrobacter rodentium*. *Nat. Immunol.* 12: 941–948.
21. Berry, D., C. Schwab, G. Milinovich, J. Reichert, K. Ben Mahfoudh, T. Decker, M. Engel, B. Hai, E. Hainzl, S. Heider, et al. 2012. Phylotype-level 16S rRNA analysis reveals new bacterial indicators of health state in acute murine colitis. *ISME J.* 6: 2091–2106.
22. Han, X., X. Ren, I. Jurickova, K. Groschwitz, B. A. Pasternak, H. Xu, T. A. Wilson, S. P. Hogan, and L. A. Denson. 2009. Regulation of intestinal barrier function by signal transducer and activator of transcription 5b. *Gut* 58: 49–58.
23. Han, X., B. Osuntokun, N. Benight, K. Loesch, S. J. Frank, and L. A. Denson. 2006. Signal transducer and activator of transcription 5b promotes mucosal tolerance in pediatric Crohn's disease and murine colitis. *Am. J. Pathol.* 169: 1999–2013.
24. Schwab, C., D. Berry, I. Rauch, I. Rennisch, J. Ramesmayer, E. Hainzl, S. Heider, T. Decker, L. Kenner, M. Müller, et al. 2014. Longitudinal study of murine microbiota activity and interactions with the host during acute inflammation and recovery. *ISME J.* 8: 1101–1114.
25. Strobl, B., I. Bubic, U. Bruns, R. Steinborn, R. Lajko, T. Kolbe, M. Karaghiosoff, U. Kalinke, S. Jonjic, and M. Müller. 2005. Novel functions of tyrosine kinase 2 in the antiviral defense against murine cytomegalovirus. *J. Immunol.* 175: 4000–4008.
26. Cash, H. L., C. V. Whitham, C. L. Behrendt, and L. V. Hooper. 2006. Symbiotic bacteria direct expression of an intestinal bactericidal lectin. *Science* 313: 1126–1130.
27. Mundy, R., T. T. MacDonald, G. Dougan, G. Frankel, and S. Wiles. 2005. *Citrobacter rodentium* of mice and man. *Cell. Microbiol.* 7: 1697–1706.
28. Wiles, S., S. Clare, J. Harker, A. Huett, D. Young, G. Dougan, and G. Frankel. 2004. Organ specificity, colonization and clearance dynamics in vivo following oral challenges with the murine pathogen *Citrobacter rodentium*. *Cell. Microbiol.* 6: 963–972.
29. Gibson, D. L., M. Montero, M. J. Ropeleski, K. S. Bergstrom, C. Ma, S. Ghosh, H. Merkens, J. Huang, L. E. Månsson, H. P. Sham, et al. 2010. Interleukin-11 reduces TLR4-induced colitis in TLR2-deficient mice and restores intestinal STAT3 signaling. *Gastroenterology* 139: 1277–1288.
30. Zhang, R., S. Gilbert, X. Yao, J. Vallance, K. Steinbrecher, R. Moriggl, D. Zhang, M. Eluri, H. Chen, H. Cao, et al. 2015. Natural compound methyl protodioscin protects against intestinal inflammation through modulation of intestinal immune responses. *Pharmacol. Res. Perspect.* 3: e00118.
31. Maxwell, J. R., and J. L. Viney. 2009. Overview of mouse models of inflammatory bowel disease and their use in drug discovery. *Curr. Protoc. Pharmacol.* Chapter 5: Unit 5.57. doi:10.1002/0471141755.ph0557s47.
32. Sugimoto, K. 2008. Role of STAT3 in inflammatory bowel disease. *World J. Gastroenterol.* 14: 5110–5114.
33. Ito, R., M. Shin-Ya, T. Kishida, A. Urano, R. Takada, J. Sakagami, J. Imanishi, M. Kita, Y. Ueda, Y. Iwakura, et al. 2006. Interferon-γ is causatively involved in experimental inflammatory bowel disease in mice. *Clin. Exp. Immunol.* 146: 330–338.
34. Kühn, R., J. Löhler, D. Rennick, K. Rajewsky, and W. Müller. 1993. Interleukin-10-deficient mice develop chronic enterocolitis. *Cell* 75: 263–274.
35. Pickert, G., C. Neufert, M. Leppkes, Y. Zheng, N. Wittkopf, M. Warntjen, H. A. Lehr, S. Hirth, B. Weigmann, S. Wirtz, et al. 2009. STAT3 links IL-22 signaling in intestinal epithelial cells to mucosal wound healing. *J. Exp. Med.* 206: 1465–1472.
36. Cox, J. H., N. M. Kljavin, N. Ota, J. Leonard, M. Roose-Girma, L. Diehl, W. Ouyang, and N. Ghilardi. 2012. Opposing consequences of IL-23 signaling mediated by innate and adaptive cells in chemically induced colitis in mice. *Mucosal Immunol.* 5: 99–109.
37. Dudakov, J. A., A. M. Hanash, and M. R. van den Brink. 2015. Interleukin-22: immunobiology and pathology. *Annu. Rev. Immunol.* 33: 747–785.
38. Mizoguchi, A., and E. Mizoguchi. 2008. Inflammatory bowel disease, past, present and future: lessons from animal models. *J. Gastroenterol.* 43: 1–17.
39. Gerdes, J., H. Lemke, H. Baisch, H. H. Wacker, U. Schwab, and H. Stein. 1984. Cell cycle analysis of a cell proliferation-associated human nuclear antigen defined by the monoclonal antibody Ki-67. *J. Immunol.* 133: 1710–1715.
40. Zheng, Y., P. A. Valdez, D. M. Danilenko, Y. Hu, S. M. Sa, Q. Gong, A. R. Abbas, Z. Modrusan, N. Ghilardi, F. J. de Sauvage, and W. Ouyang. 2008. Interleukin-22 mediates early host defense against attaching and effacing bacterial pathogens. *Nat. Med.* 14: 282–289.
41. Jostins, L., S. Ripke, R. K. Weersma, R. H. Duerr, D. P. McGovern, K. Y. Hui, J. C. Lee, L. P. Schumm, Y. Sharma, C. A. Anderson, et al; International IBD Genetics Consortium (IIBDGC). 2012. Host-microbe interactions have shaped the genetic architecture of inflammatory bowel disease. *Nature* 491: 119–124.
42. Ishizaki, M., T. Akimoto, R. Muromoto, M. Yokoyama, Y. Ohshiro, Y. Sekine, H. Maeda, K. Shimoda, K. Oritani, and T. Matsuda. 2011. Involvement of tyrosine kinase-2 in both the IL-12/Th1 and IL-23/Th17 axes in vivo. *J. Immunol.* 187: 181–189.
43. Oyamada, A., H. Ikebe, M. Itsumi, H. Saiwai, S. Okada, K. Shimoda, Y. Iwakura, K. I. Nakayama, Y. Iwamoto, Y. Yoshikai, and H. Yamada. 2009. Tyrosine kinase 2 plays critical roles in the pathogenic CD4 T cell responses for the development of experimental autoimmune encephalomyelitis. *J. Immunol.* 183: 7539–7546.
44. Sugimoto, K., A. Ogawa, E. Mizoguchi, Y. Shimomura, A. Andoh, A. K. Bhan, R. S. Blumberg, R. J. Xavier, and A. Mizoguchi. 2008. IL-22 ameliorates intestinal inflammation in a mouse model of ulcerative colitis. *J. Clin. Invest.* 118: 534–544.
45. Zenewicz, L. A., G. D. Yancopoulos, D. M. Valenzuela, A. J. Murphy, S. Stevens, and R. A. Flavell. 2008. Innate and adaptive interleukin-22 protects mice from inflammatory bowel disease. *Immunity* 29: 947–957.
46. Melgar, S., A. Karlsson, and E. Michaëlsson. 2005. Acute colitis induced by dextran sulfate sodium progresses to chronicity in C57BL/6 but not in BALB/c mice: correlation between symptoms and inflammation. *Am. J. Physiol. Gastrointest. Liver Physiol.* 288: G1328–G1338.
47. Hildebrand, F., T. L. Nguyen, B. Brinkman, R. G. Yunta, B. Cauwe, P. Vandenabeele, A. Liston, and J. Raes. 2013. Inflammation-associated enterotypes, host genotype, cage and inter-individual effects drive gut microbiota variation in common laboratory mice. *Genome Biol.* 14: R4.
48. te Velde, A. A., M. I. Verstege, and D. W. Hommes. 2006. Critical appraisal of the current practice in murine TNBS-induced colitis. *Inflamm. Bowel Dis.* 12: 995–999.
49. Smith, C. L., T. L. Arvedson, K. S. Cooke, L. J. Dickmann, C. Forte, H. Li, K. L. Merriam, V. K. Perry, L. Tran, J. B. Rottman, and J. R. Maxwell. 2013. IL-22 regulates iron availability in vivo through the induction of hepcidin. *J. Immunol.* 191: 1845–1855.
50. Zindl, C. L., J. F. Lai, Y. K. Lee, C. L. Maynard, S. N. Harbour, W. Ouyang, D. D. Chaplin, and C. T. Weaver. 2013. IL-22-producing neutrophils contribute to antimicrobial defense and restitution of colonic epithelial integrity during colitis. *Proc. Natl. Acad. Sci. USA* 110: 12768–12773.
51. Neufert, C., G. Pickert, Y. Zheng, N. Wittkopf, M. Warntjen, A. Nikolaev, W. Ouyang, M. F. Neurath, and C. Becker. 2010. Activation of epithelial STAT3 regulates intestinal homeostasis. *Cell Cycle* 9: 652–655.
52. Diegelmann, J., T. Olszak, B. Göke, R. S. Blumberg, and S. Brand. 2012. A novel role for interleukin-27 (IL-27) as mediator of intestinal epithelial barrier protection mediated via differential signal transducer and activator of transcription (STAT) protein signaling and induction of antibacterial and anti-inflammatory proteins. *J. Biol. Chem.* 287: 286–298.
53. Lejeune, D., L. Dumoutier, S. Constantinescu, W. Kruijer, J. J. Schuringa, and J. C. Renauld. 2002. Interleukin-22 (IL-22) activates the JAK/STAT, ERK, JNK, and p38 MAP kinase pathways in a rat hepatoma cell line. Pathways that are shared with and distinct from IL-10. *J. Biol. Chem.* 277: 33676–33682.
54. Rendon, J. L., X. Li, S. Akhtar, and M. A. Choudhry. 2013. Interleukin-22 modulates gut epithelial and immune barrier functions following acute alcohol exposure and burn injury. *Shock* 39: 11–18.
55. Collins, J. W., K. M. Keeney, V. F. Crepin, V. A. Rathinam, K. A. Fitzgerald, B. B. Finlay, and G. Frankel. 2014. *Citrobacter rodentium*: infection, inflammation and the microbiota. *Nat. Rev. Microbiol.* 12: 612–623.
56. Wittkopf, N., G. Pickert, U. Billmeier, M. Mahapatro, S. Wirtz, E. Martini, M. Leppkes, M. F. Neurath, and C. Becker. 2015. Activation of intestinal epithelial Stat3 orchestrates tissue defense during gastrointestinal infection. *PLoS One* 10: e0118401.

57. Brown, E. M., M. Sadarangani, and B. B. Finlay. 2013. The role of the immune system in governing host-microbe interactions in the intestine. *Nat. Immunol.* 14: 660–667.
58. Garrett, W. S., C. A. Gallini, T. Yatsunenko, M. Michaud, A. DuBois, M. L. Delaney, S. Punit, M. Karlsson, L. Bry, J. N. Glickman, et al. 2010. Enterobacteriaceae act in concert with the gut microbiota to induce spontaneous and maternally transmitted colitis. *Cell Host Microbe* 8: 292–300.
59. Lupp, C., M. L. Robertson, M. E. Wickham, I. Sekirov, O. L. Champion, E. C. Gaynor, and B. B. Finlay. 2007. Host-mediated inflammation disrupts the intestinal microbiota and promotes the overgrowth of Enterobacteriaceae. *Cell Host Microbe* 2: 119–129.
60. Zenewicz, L. A., X. Yin, G. Wang, E. Elinav, L. Hao, L. Zhao, and R. A. Flavell. 2013. IL-22 deficiency alters colonic microbiota to be transmissible and colitogenic. *J. Immunol.* 190: 5306–5312.
61. Behnsen, J., S. Jellbauer, C. P. Wong, R. A. Edwards, M. D. George, W. Ouyang, and M. Raffatellu. 2014. The cytokine IL-22 promotes pathogen colonization by suppressing related commensal bacteria. *Immunity* 40: 262–273.
62. Eken, A., A. K. Singh, P. M. Treuting, and M. Oukka. 2014. IL-23R$^+$ innate lymphoid cells induce colitis via interleukin-22-dependent mechanism. *Mucosal Immunol.* 7: 143–154.
63. Willson, T. A., I. Jurickova, M. Collins, and L. A. Denson. 2013. Deletion of intestinal epithelial cell STAT3 promotes T-lymphocyte STAT3 activation and chronic colitis following acute dextran sodium sulfate injury in mice. *Inflamm. Bowel Dis.* 19: 512–525.
64. Lian, L. H., T. P. Lau, V. L. Lee, W. S. Lee, I. Hilmi, K. L. Goh, and K. H. Chua. 2013. Lack of association between TYK2 and STAT3 genes and Crohn's disease in the Malaysian population. *Genet. Mol. Res.* 12: 167–174.
65. Sohn, S. J., K. Barrett, A. Van Abbema, C. Chang, P. B. Kohli, H. Kanda, J. Smith, Y. Lai, A. Zhou, B. Zhang, et al. 2013. A restricted role for TYK2 catalytic activity in human cytokine responses revealed by novel TYK2-selective inhibitors. *J. Immunol.* 191: 2205–2216.
66. Works, M. G., F. Yin, C. C. Yin, Y. Yiu, K. Shew, T. T. Tran, N. Dunlap, J. Lam, T. Mitchell, J. Reader, et al. 2014. Inhibition of TYK2 and JAK1 ameliorates imiquimod-induced psoriasis-like dermatitis by inhibiting IL-22 and the IL-23/IL-17 axis. *J. Immunol.* 193: 3278–3287.